



Title	GeSn/SiGeSn Multiple-Quantum-Well Electroabsorption Modulator With Taper Coupler for Mid-Infrared Ge-on-Si Platform
Author(s)	Akie, Minami; Fujisawa, Takeshi; Sato, Takanori; Arai, Masakazu; Saitoh, Kunimasa
Citation	IEEE journal of selected topics in quantum electronics, 24(6), 3400208 https://doi.org/10.1109/JSTQE.2018.2827673
Issue Date	2018-11
Doc URL	http://hdl.handle.net/2115/70800
Rights	© 2018 IEEE. Personal use of this material is permitted. Permission from IEEE must be obtained for all other uses, in any current or future media, including reprinting/republishing this material for advertising or promotional purposes, creating new collective works, for resale or redistribution to servers or lists, or reuse of any copyrighted component of this work in other works.
Type	article (author version)
File Information	JSTQE_final submitted.pdf



[Instructions for use](#)

GeSn/SiGeSn Multiple-Quantum-Well Electroabsorption Modulator with Taper Coupler for Mid-Infrared Ge-on-Si platform

Minami Akie, Takeshi Fujisawa, Member IEEE, Takanori Sato,
Masakazu Arai, and Kunimasa Saitoh, Member IEEE

Abstract— We propose taper coupler electroabsorption modulator (EAM) composed of GeSn/SiGeSn multiple-quantum-well (MQW) on Ge-on-Si platform for mid-infrared (2 μm) integrated optical active devices. The epitaxial design is performed by calculating the absorption spectra of GeSn/SiGeSn MQW using many-body theory to investigate the extinction characteristics of GeSn MQW waveguides. Two types of taper couplers are considered for connecting Ge-rib waveguide and GeSn-MQW-highmesa waveguide efficiently. One is an adiabatic taper coupler type EAM (ATC type EAM) and it is useful for thin Ge-buffer structure in terms of the extinction ratio. Another is a resonant taper coupler type EAM (RTC type EAM) and it is superior to ATC type EAM for thick Ge-buffer. It is confirmed that RTC type EAM can obtain the high extinction characteristics with low-loss and shorter device length (6.87 dB, -3.97 dB, and 215 μm) compared with conventional ATC type EAM for thick Ge-buffer (5.67 dB, -4.9 dB, and 340 μm).

Index Terms— Mid-infrared photonics, GeSn quantum wells

I. INTRODUCTION

MID-INFRARED (mid-IR) band (1.8 ~ 5.0 μm) is now attracting considerable attention for sensing and optical communication applications [1]. In particular, 1.95 μm is the minimum attenuation wavelength of the hollow-core photonic bandgap fiber [2], which is expected as a new wavelength band to increase the transmission capacity. For the mid-IR devices, Ge-on-Si platform is suitable due to its wider low-loss spectrum spanning from 1.8 to 14 μm and its CMOS compatibility for mid-IR photonic integration [1], [3]. A variety of active and passive devices have been developed for this platform.

For active components, the active region (either bulk or quantum well) is grown on Ge-buffer layer. For example, strong electroabsorption (EA) based on quantum-confined Stark effect (QCSE) in the Ge/SiGe multiple quantum well (MQW) was

observed in [4] around 1.45 μm . The wavelength range can be extended to mid-IR region by incorporating small amount of Sn to Ge [5]. Recently, GeSn lasers emitting 2- μm wavelength range light have been experimentally realized [6-10]. In future, the monolithic integration of various components will be required for increasing the functionality of the chip. Other important active component is an electroabsorption (EA) device. EA devices can be used for various optical signal processing, such as switching, and one of the most important application is an EA modulator (EAM) due to its high-speed characteristics. EAMs and lasers can be (in principle) monolithically integrated, and therefore, an on-chip optical communication may be possible by integrating all the components (lasers, modulators, and detectors) on the same Si chip by using mid-IR wavelengths. However, there are few reports of EAM based on group IV material for 2- μm wavelength range.

Usually, active layers are grown on Ge-buffer layer with the typical thickness of several microns [6]. The thickness of the buffer layer depends on various factors: desired crystal quality of active regions, the limitation of growth technologies, etc. For passive components, Ge-rib waveguides are useful and various passive components have been fabricated [11]. Therefore, in the integrated chip, optical signal should be routed by the passive Ge-rib waveguide and access to the highmesa active waveguide, on demand. One approach is to use taper coupler [12-14] for efficient coupling between the GeSn active device and passive waveguides. The taper coupler is an important approach to achieve efficient vertical coupling between layers. There are two types of taper coupler: an adiabatic taper coupler and a resonant taper coupler. The adiabatic taper coupler is a structure that avoids the power transfer from the fundamental mode to higher-order and radiation modes. One problem in adiabatic taper coupler type electroabsorption modulator (ATC type EAM) is that the confinement factor of the fundamental mode (E_{11}) in the MQW active region becomes very small if thick Ge-buffer layer is used, because the majority of the power lies in Ge-rib region in highmesa waveguide, leading to poor performance of active devices. To overcome this limitation, we reported the resonant taper coupler type EAM (RTC type EAM) in the preliminary conference proceedings [15]. The advantage of the RTC type EAM is to use vertical multimode interference between E_{11} and E_{12} modes. As shown later, since E_{12} mode has larger field overlap with MQW active region, extinction

Manuscript received January 31, 2018.

M. Akie, T. Sato, T. Fujisawa, and K. Saitoh are with the Graduate School of Information Science and Technology, Hokkaido University, Sapporo 060-0814, Japan (e-mail: akie@icp.ist.hokudai.ac.jp; tsato@icp.ist.hokudai.ac.jp; fujisawa@ist.hokudai.ac.jp; ksaitoh@ist.hokudai.ac.jp).

M. Arai is with the Department of Applied Physics and Electronic Engineering, University of Miyazaki, Miyazaki, 889-2192, Japan (e-mail: arai.masakazu@cc.miyazaki-u.ac.jp)

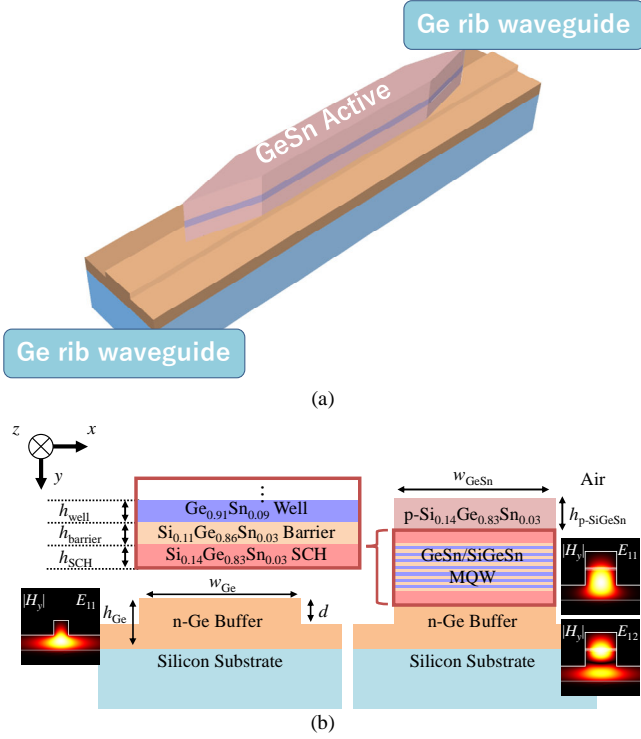


Fig. 1. (a) The schematic of proposed EAM with a taper coupler and (b) cross sections of Ge-rib (left) and GeSn MQW highmesa waveguides (right).

Material	Refractive index
Air	1.000
Si	3.455
Ge	4.110
p-Si _{0.14} Ge _{0.83} Sn _{0.03}	4.055
Si _{0.14} Ge _{0.83} Sn _{0.03} SCH	4.055
Si _{0.11} Ge _{0.86} Sn _{0.03} barrier	4.046
Ge _{0.91} Sn _{0.09} well	4.193

characteristics are improved. However, ATC type EAM will be superior for thin Ge-buffer because the confinement factor of E_{11} mode in MQW region will be large. As written above, since the thickness of the buffer layer depends on various conditions, optimum device structures for active-passive integration will be changed depending on the buffer thickness.

In this paper, we propose taper coupler EAM composed of GeSn/SiGeSn MQW on Ge-on-Si platform for mid-infrared (2 μm) integrated optical active devices. GeSn/SiGeSn QW design for 2- μm band QCSE is done for the first time and the epitaxial design is performed by calculating the absorption spectra of GeSn/SiGeSn MQW using many-body theory developed for group IV materials [16,17] to investigate the extinction characteristics of GeSn MQW waveguides. Two types of taper couplers are considered for connecting Ge-rib waveguide and GeSn-MQW-highmesa waveguide efficiently and comprehensive comparison of two structures, ATC type EAM

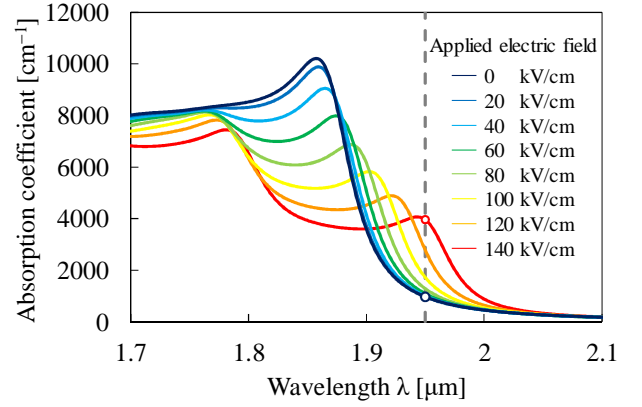


Fig. 2. Absorption spectra of the GeSn/SiGeSn QW calculated by MBT (TE polarization).

and RTC type EAM, is done. It is confirmed that RTC type EAM can obtain the high extinction characteristics with shorter device length compared with conventional ATC type EAM for thick Ge-buffer.

II. QW STRUCTURE AND MQW WAVEGUIDE

A. Absorption Spectra of GeSn/SiGeSn MQW

Figure 1 (a) shows the three-dimensional structure of proposed EAM with taper coupler. It consists of Ge-rib input/output waveguide and GeSn MQW highmesa waveguide. These two waveguides are connected via taper coupler as shown in the Figure. This type of two-step waveguide structure was recently fabricated [14]. Figure 1 (b) shows the cross sections of Ge-rib and GeSn/SiGeSn MQW highmesa waveguides, considered here. The insets show the field distributions of E_{11} and E_{12} modes. The waveguide parameters shown in Fig. 1 are given as follows: $h_{\text{p-SiGeSn}} = 1.0 \mu\text{m}$, $h_{\text{well}} = 0.01 \mu\text{m}$, $h_{\text{barrier}} = 0.01 \mu\text{m}$, $h_{\text{SCH}} = 0.045 \mu\text{m}$, where $h_{\text{p-SiGeSn}}$, h_{well} , h_{barrier} , and h_{SCH} denote the height of p-SiGeSn layer, well layer, barrier layer, and separate-confinement heterostructures (SCH) layer, respectively. 10^{18} and 10^{17} cm^{-3} doping concentrations are assumed for n- and p-cladding layers [18]. We assume the loss originating from free-carrier absorption and other effects in these layers in beam propagation simulation. The loss values are extracted from [19] and they are 3 and 10 cm^{-1} for n- and p-cladding layers at 1.95 μm . Although p-cladding is SiGeSn, we used the loss value for Ge. This is because that the loss of Si [20] is smaller than Ge.

The refractive indexes of each layer are summarized in Table I. The GeSn/SiGeSn MQW is grown on the Ge-buffer consists of 10 layers of the Ge_{0.91}Sn_{0.09} well and the Si_{0.11}Ge_{0.86}Sn_{0.03} barrier. The QWs are sandwiched by two Si_{0.14}Ge_{0.83}Sn_{0.03} SCH and grown on the doped n-Ge buffer on Si substrate. The composition of the barrier and SCH layers are lattice matched to the Ge-buffer and have bandgap wavelength of 1.2 and 1.15 μm . Here, we consider 2- μm band communication application. The operating wavelength of EAM is set to 1.95 μm , which is the lowest loss wavelength of photonic bandgap fiber [2]. The well is Ge_{0.91}Sn_{0.09} with 1.3% compressive strain, whose bandgap

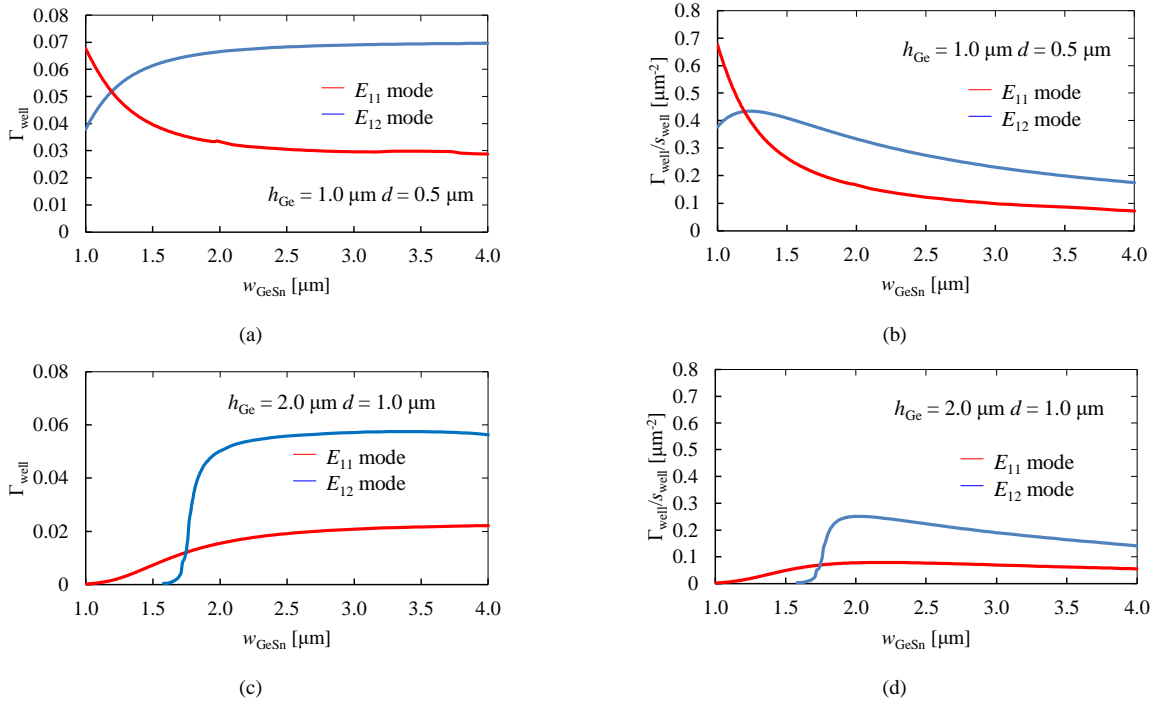


Fig. 3. (a) Γ_{well} and (b) $\Gamma_{\text{well}}/s_{\text{well}}$ with $h_{\text{Ge}} = 1.0 \mu\text{m}$, (c) Γ_{well} and (d) $\Gamma_{\text{well}}/s_{\text{well}}$ with $h_{\text{Ge}} = 2.0 \mu\text{m}$ as a function of w_{GeSn} for E_{11} and E_{12} modes calculated by VFEM.

wavelength is $1.85 \mu\text{m}$ without bias. Therefore, the detuning is 100 nm . The composition of the barrier and SCH layers are determined to maximize the depth of the well in conduction band with the condition of zero strain to Ge-buffer. Deep well leads to stronger electron confinement and steep extinction characteristics [17]. The material parameters, such as lattice constant and bandgap, used in this paper are the same as [16] and [17]. Figure 2 shows the calculated absorption spectra (TE polarization) of the GeSn/SiGeSn QW by MBT for various values of applied electric fields. Red shift of spectra due to QCSE can be seen. For calculating these spectra, inhomogeneous broadening with the broadening energy of $\gamma = 7.5 \text{ meV}$ is taken into account [17]. In [17], it was shown that calculated absorption spectra of Ge/SiGe QWs are in very good agreement with the measurement [4], showing the validity of the method for quantifying the absorption spectra of group IV QWs. The absorption spectra shown in Fig. 2 is used for the EAM analysis. Since the thickness of the insulating layer is 300 nm , the voltage corresponding to 140 kV/cm is 4.2 V . It should be noted that QCSE in $2\text{-}\mu\text{m}$ wavelength range was experimentally confirmed for InP-based material [21]. Also, it is possible to extend the operating wavelength to longer wavelength region by using GeSn buffer layer.

B. Confinement Factor in QW Region

In order to obtain high ER and to reduce the device size, it is necessary to increase confinement factor in the QW region (Γ_{well}). We investigate Γ_{well} when waveguide width and height are changed for different thickness of Ge-buffer (h_{Ge}). Figures 3(a)-(d) show Γ_{well} and $\Gamma_{\text{well}}/s_{\text{well}}$ of E_{11} and E_{12} modes as a

function of w_{GeSn} for $h_{\text{Ge}} = 1.0$ and $2.0 \mu\text{m}$, where s_{well} is the area of all well layers. Γ_{well} is calculated by vectorial finite element method (VFEM) [22]. We can see that E_{12} mode has larger field overlap with the MQW active region for $h_{\text{Ge}} = 2.0 \mu\text{m}$. In contrast, Γ_{well} of fundamental mode (E_{11}) is larger than that of E_{12} modes for $h_{\text{Ge}} = 1.0 \mu\text{m}$. Γ_{well} of the fundamental mode (E_{11}) in the active region is very small for thick Ge-buffer layer since the majority of the power lies in Ge-rib region in GeSn MQW highmesa waveguide. Accordingly, if h_{Ge} is $1 \mu\text{m}$, ATC type EAM can reduce size and obtain high ER, but if h_{Ge} is $2.0 \mu\text{m}$, the performance of ATC type EAM deteriorates because Γ_{well} of E_{11} mode becomes small. For $h_{\text{Ge}} = 2.0 \mu\text{m}$, it is better to use RTC type EAM as shown in the next section.

For the electrical connection, heavy-doped p-contacting layer and metal film on the p-cladding are necessary. However, if there is a 100-nm p-contacting layer on the $1\text{-}\mu\text{m}$ p-cladding layer, the confinement factor of E_{12} mode is below 0.5% . Therefore, they are neglected in this paper.

III. EFFICIENT CONNECTING STRUCTURE AND THE EXTINCTION CHARACTERISTICS

Here, we discuss two types of taper couplers. Operating wavelength is $1.95 \mu\text{m}$ and imaginary part of refractive index is deduced from the absorption coefficient α shown in Fig. 2 by following equation:

$$n_{\text{im}} = -\frac{\alpha\lambda}{4\pi}. \quad (1)$$

Long and gentle taper is required ($> 40 \mu\text{m}$) for the adiabatic taper coupler because the power transfer from fundamental

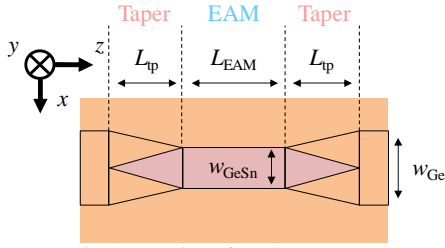


Fig. 4. Top view of ATC type EAM.

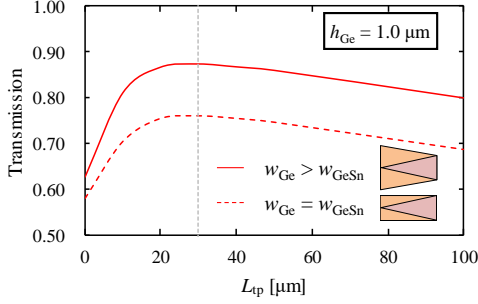


Fig. 5. Transmission in taper region as a function of L_{tp1} for $h_{Ge} = 1.0 \mu\text{m}$.

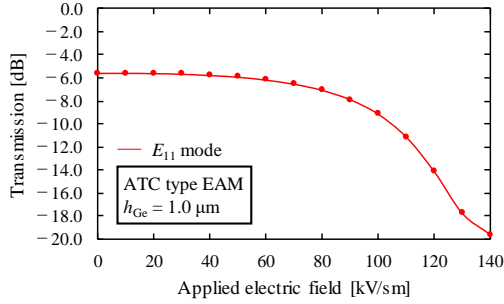


Fig. 6. ER as a function of applied electric field of ATC type EAM with $h_{Ge} = 1.0 \mu\text{m}$.

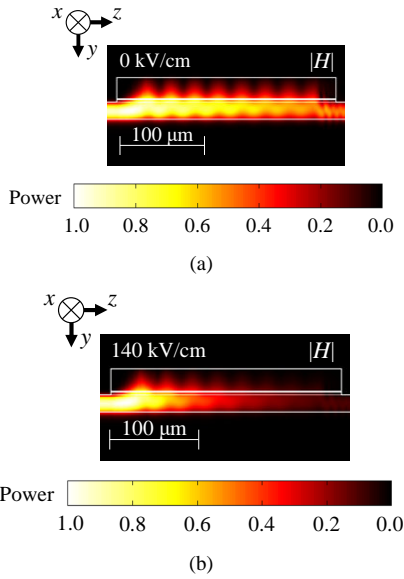


Fig. 7. $|H|$ distribution (yz -plane) of ATC type EAM with $h_{Ge} = 1.0 \mu\text{m}$ (a) at applied electric field of 0 kV/cm and (b) at applied electric field of 140 kV/cm.

mode to higher-order and radiation modes should be avoided. On the contrary, for the resonant taper coupler, very short taper

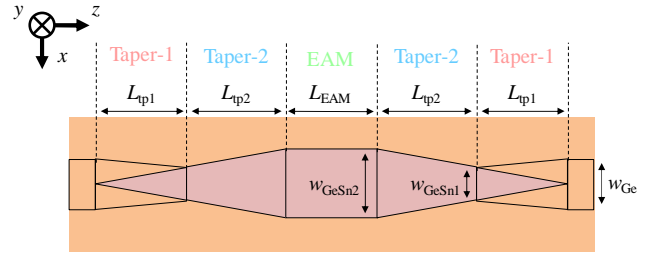


Fig. 8. Top view of ATC type EAM for $h_{Ge} = 2.0 \mu\text{m}$.

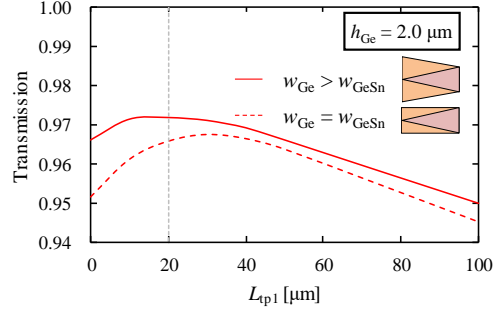


Fig. 9. Transmission in taper-1 region as a function of L_{tp1} for $h_{Ge} = 2.0 \mu\text{m}$

length ($< 10 \mu\text{m}$) is used to excite both fundamental and higher-order modes. Properly adjusting waveguide length corresponding to the beat length of multimode interference, E_{11} mode can be extracted from the output. In following section, we investigate the transmission and extinction ratio (ER) characteristics of ATC type EAM and RTC type EAM. Both analyses are performed by vectorial finite element beam propagation method (VFE-BPM) [23,24].

A. ATC Type EAM

Here, we consider ATC type EAM for smoothly connecting Ge-rib and GeSn highmesa waveguides. First, we describe the case of $h_{Ge} = 1.0 \mu\text{m}$ (thin Ge-buffer). Figure 4 shows the top-view of ATC type EAM. It consists of two sections: Ge-rib and highmesa taper (taper) and EAM. From Fig. 3(b), we select $w_{GeSn} = 1.2 \mu\text{m}$ because maximum value of Γ_{well}/s_{well} is obtained at $w_{GeSn} = 1.2 \mu\text{m}$. In the taper, the Ge-rib waveguide is adiabatically connected to the GeSn highmesa waveguide for avoiding the power transfer from fundamental mode to higher order and radiation modes. Figure 5 shows transmission of taper section as a function of L_{tp} at $h_{Ge} = 1.0 \mu\text{m}$. Solid line is the transmission for $w_{Ge} = 1.97 \mu\text{m} > w_{GeSn}$. For these widths, the effective indexes of E_{11} mode in Ge-rib and E_{11} mode in highmesa waveguides are matched. Dashed line shows the transmission for $w_{Ge} = w_{GeSn}$. For the calculation, the absorption coefficient at $1.95 \mu\text{m}$ and 0 kV/cm (no bias) is assumed in the QW region. Since the effective refractive index of GeSn MQW waveguide is different from that of the Ge-rib waveguide, the connection of the waveguide with the same width raises the coupling loss. Accordingly, the transmission is slightly improved by adjusting effective refractive index of the GeSn MQW waveguide to that of the Ge-rib waveguide. If the taper length is too short, the transmission decreases due to radiation

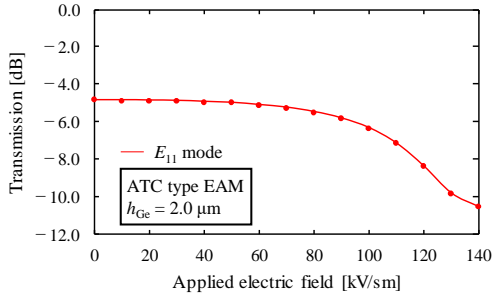


Fig. 10. ER as a function of applied electric field of ATC type EAM with $h_{\text{Ge}} = 2.0 \mu\text{m}$.

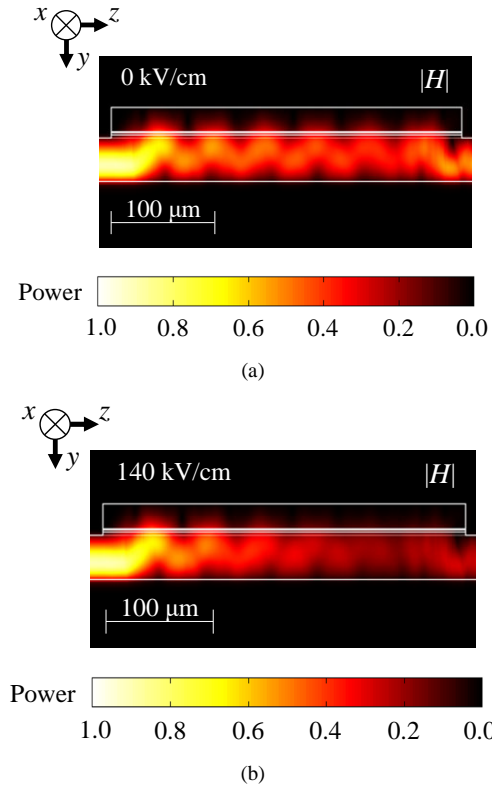


Fig. 11. $|H|$ distribution (yz -plane) of ATC type EAM with $h_{\text{Ge}} = 2.0 \mu\text{m}$ (a) at applied electric field of 0 kV/cm and (b) at applied electric field of 140 kV/cm.

loss and coupling to higher-order mode. Even if the taper length is long, loss due to the QW absorption at the taper section increases. The maximum transmission is obtained at $L_{\text{tp}} = 30 \mu\text{m}$. Figure 6 shows the ER as a function of applied electric field and Figs. 7(a) and (b) show $|H|$ -field distribution in yz -plane at the center of the waveguide of ATC type EAM with $h_{\text{Ge}} = 1.0 \mu\text{m}$ at applied electric field of 0 kV/cm and 140 kV/cm. We assumed that the electric field is applied to only EAM section in Fig. 4. The electric field can be selectively applied to the EAM region by removing the p-contacting layer on the p-cladding in the taper region. L_{EAM} is set to 200 μm . ATC type EAM with $h_{\text{Ge}} = 1.0 \mu\text{m}$ has ER of 14.0 dB between 0 kV/cm and 140 kV/cm and the insertion loss at 0 kV/cm is -5.56 dB . The total length including taper is 260 μm .

Next, we describe the case of $h_{\text{Ge}} = 2.0 \mu\text{m}$. Figure 8 shows

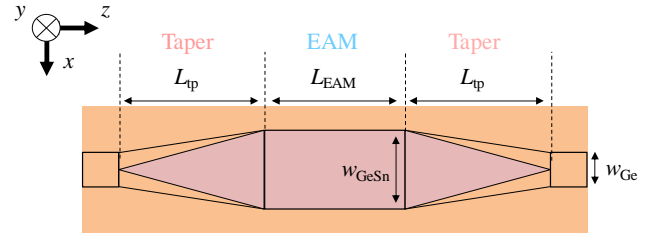


Fig. 12. Top view of RTC type EAM.

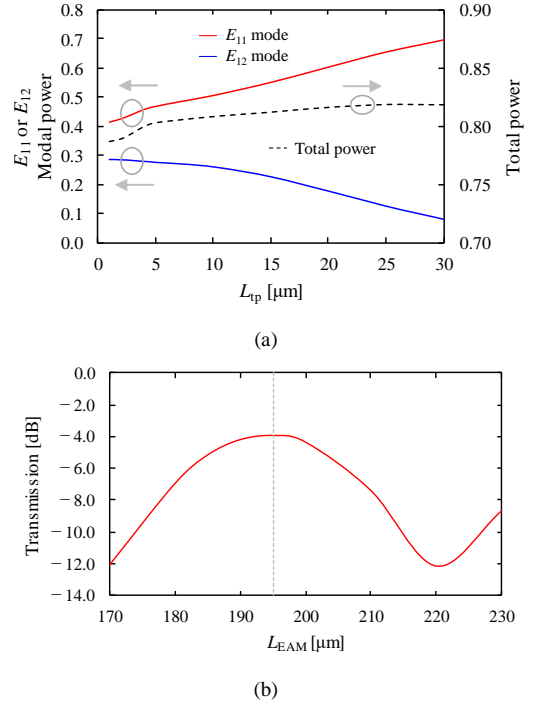


Fig. 13. (a) E_{11} and E_{12} mode power as a function of the taper length L_{tp} and (b) output power of E_{11} mode of Ge-rib waveguide of proposed EAM for $L_{\text{tp}1} = 10 \mu\text{m}$ as a function of L_{EAM} .

the structure of ATC type EAM with $h_{\text{Ge}} = 2.0 \mu\text{m}$. It consists of three sections: Ge-rib and highmesa taper (taper-1), highmesa taper (taper-2), and EAM. Figure 9 shows transmission of taper-1 as a function of $L_{\text{tp}1}$ at $h_{\text{Ge}} = 2.0 \mu\text{m}$, where $w_{\text{Ge}} = 1.4 \mu\text{m}$, $d = 1.0 \mu\text{m}$. As in Fig. 9, the solid line is the transmission for $w_{\text{Ge}} > w_{\text{GeSn}1} = 1.34 \mu\text{m}$. For these widths, the effective indexes of E_{11} mode in Ge-rib and E_{11} mode in highmesa waveguides are matched. The dashed line shows the transmission for $w_{\text{Ge}} = w_{\text{GeSn}1}$. Similar to the structure of $h_{\text{Ge}} = 1.0 \mu\text{m}$, the transmission is improved by adjusting effective refractive index of the GeSn MQW waveguide to that of the Ge-rib waveguide. Maximum transmission is obtained around $L_{\text{tp}1} = 20 \mu\text{m}$. According to Fig. 3 (c), since the confinement factor of E_{11} mode is below 1% for $w_{\text{GeSn}1} = 1.34 \mu\text{m}$, the waveguide width is further tapered to $w_{\text{GeSn}2}$ to increase the confinement factor. From Fig. 3(c), we select $w_{\text{GeSn}2} = 4.0 \mu\text{m}$, where Γ_{well} of E_{11} is saturated to w_{GeSn} and the value is 2.2%. From above discussion, taper parameters are determined as follows: $w_{\text{Ge}} = 1.4 \mu\text{m}$, $d = 1.0 \mu\text{m}$, $w_{\text{GeSn}1} = 1.34 \mu\text{m}$, $w_{\text{GeSn}2} = 4.0 \mu\text{m}$, $L_{\text{tp}1} = 20 \mu\text{m}$. $L_{\text{tp}2}$ is set 50 μm , at which the transmission of E_{11} mode is maximized. L_{EAM} is set to

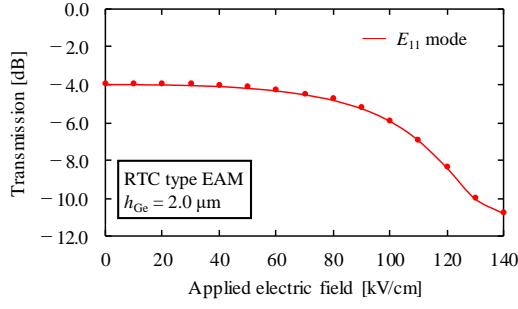


Fig. 14. ER as a function of applied electric field of the EAM using the RTC type EAM with $h_{\text{Ge}} = 2.0 \mu\text{m}$.

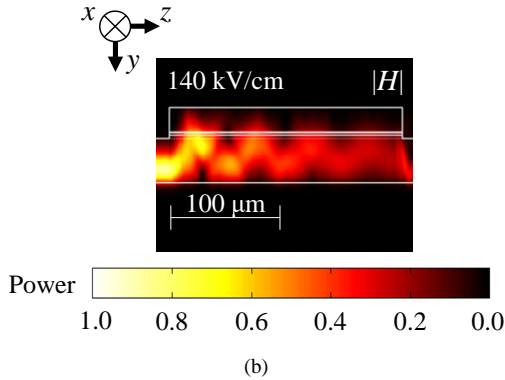
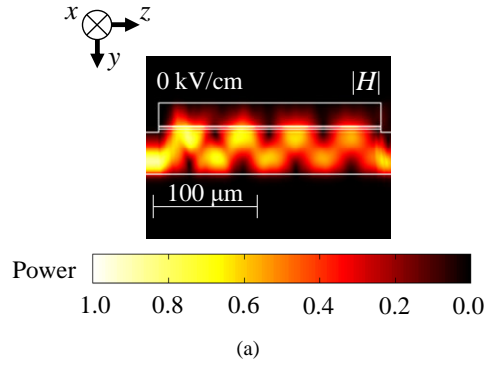


Fig. 15. $|H|$ distribution (yz -plane) of RTC type EAM with $h_{\text{Ge}} = 2 \mu\text{m}$ (a) at applied electric field of 0 kV/cm and (b) at applied electric field of 140 kV/cm.

200 μm . Figure 10 shows the ER as a function of applied electric field and Figs. 11 (a) and (b) show $|H|$ -field distributions of ATC type EAM with $h_{\text{Ge}} = 2.0 \mu\text{m}$ at applied electric field of 0 kV/cm and 140 kV/cm. We assumed that the electric field is applied to only EAM section in Fig. 8. ATC type EAM with $h_{\text{Ge}} = 2.0 \mu\text{m}$ has ER of 5.67 dB between 0 kV/cm and 140 kV/cm and the insertion loss at 0 kV/cm is -4.9 dB. Total length including taper is 340 μm .

B. RTC Type EAM

In ATC type EAM with $h_{\text{Ge}} = 2.0 \mu\text{m}$, the device size and insertion loss at 0 kV/cm are increased compared with the ATC type EAM with $h_{\text{Ge}} = 1.0 \mu\text{m}$ due to low Γ_{well} and the absorption in long taper section. For thick Ge-buffer, since the higher-order mode (E_{12}) has larger confinement factor in QW region, RTC type EAM will be superior to ATC type EAM.

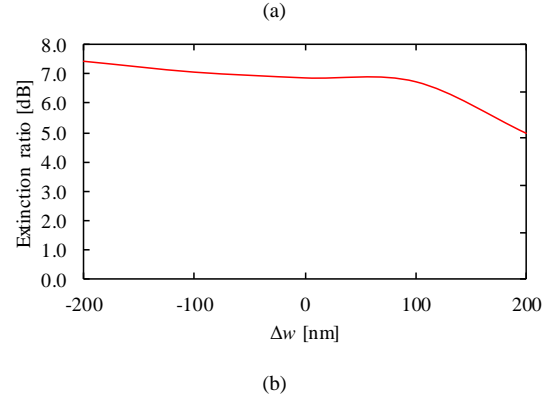
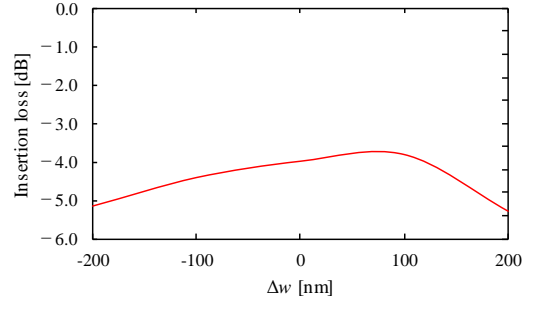


Fig. 16. (a) Insertion loss and (b) extinction ratio of RTC-type EAM as a function of Δw .

Figure 12 shows the top-view of RTC type EAM. It consists of two sections: Ge-rib and highmesa taper (taper) and EAM. We set $w_{\text{Ge}} = 1.0 \mu\text{m}$, $d = 1.0 \mu\text{m}$, and $w_{\text{GeSn}} = 2.32 \mu\text{m}$ to match the effective indexes of E_{11} mode in Ge-rib and E_{12} mode in highmesa waveguides. The confinement factor of E_{11} and E_{12} modes in the QW region of highmesa waveguide are 1.8 and 5.6%. Figure 13 (a) shows the modal power of E_{11} , E_{12} modes and total power as a function of the taper length L_{tp} . Both E_{11} and E_{12} modes are excited in the taper and we set $L_{\text{tp}} = 10 \mu\text{m}$. Figure 13 (b) shows the output power of E_{11} mode of Ge-rib waveguide of proposed EAM for $L_{\text{tp}} = 10 \mu\text{m}$ as a function of L_{EAM} (Output power of whole device including input and output tapers and EAM section). Since in the EAM section, E_{11} and E_{12} modes excited by taper section are propagated with beating, there is an optimum EAM length for maximizing the transmission of E_{11} mode of Ge-rib waveguide. As shown in Fig. 13 (b), for $L_{\text{EAM}} = 195 \mu\text{m}$, the output power is maximized. Figure 14 shows the ER as a function of applied electric field of RTC type EAM with $L_{\text{tp}} = 10 \mu\text{m}$, and $L_{\text{EAM}} = 195 \mu\text{m}$ (the total length is 215 μm) and Figs. 15 (a) and (b) show $|H|$ -field distributions of RTC type EAM with $h_{\text{Ge}} = 2.0 \mu\text{m}$ at applied electric field of 0 kV/cm and 140 kV/cm. RTC type EAM has ER of 6.87 dB between 0 kV/cm and 140 kV/cm and the insertion loss at 0 kV/cm is -3.97 dB. The increased ER compared with ATC type EAM with thick Ge-buffer comes from the use of E_{12} mode having large confinement factor, and low-loss and short device length come from the short taper length at $h_{\text{Ge}} = 2 \mu\text{m}$. Furthermore, the width and length of EAM section are 2.32 and 195 μm (half of ATC type EAM with $h_{\text{Ge}} = 2 \mu\text{m}$), which are typical waveguide width and length of

state-of-the-art high-speed EAM for telecommunication band [25]. 3-dB bandwidth (f_{3dB}) of the RTC-type EAM is estimated based on simple calculation method described in [26]. The capacitance of the active region is 0.232 pF if we assume the dielectric constant of the active region as 4.193² (the refractive index of well material). If we assume 50 Ω termination register, f_{3dB} is about 27 GHz, comparable to high-speed EAM in telecommunication band [25].

Figures 16 (a) and (b) show the insertion loss and extinction ratio of RTC type EAM as a function of Δw . Here Δw is a deviation from $w_{GeSn} = 2.32 \mu\text{m}$. Other parameters are the same with the RTC-type EAM shown in Fig. 14. From the results, 200-nm deviation in the waveguide width does not affect much to the device performance.

IV. CONCLUSION

We proposed tapered coupler EAM composed of GeSn/SiGeSn multiple-quantum-well (MQW) on Ge-on-Si platform for mid-infrared (2 μm) integrated optical active devices. We calculated the absorption spectra of GeSn/SiGeSn MQW around 2 μm by MBT, and investigated the extinction characteristics of GeSn MQW waveguides. ATC and RTC type EAMs are proposed and comprehensive comparison of these two structures are done in terms of Ge-buffer thickness. Due to the different confinement factor of the fundamental mode in QW region, ATC type EAM is useful for thin buffer and RTC type EAM is useful for thick buffer layer.

REFERENCES

- [1] R. Soref, "Mid-infrared photonics in silicon and germanium," *Nat. Photonics*, vol. 4, no. 8, pp. 495–497, Aug. 2010.
- [2] P. J. Roberts, F. Couny, H. Sabert, B. J. Mangan, D. P. Williams, L. Farr, M. W. Mason, A. Tomlinson, T. A. Birks, J. C. Knight, and P. St. J. Russell, "Ultimate low loss of hollow-core photonic crystal fibres," *Opt. Express*, vol. 13, no. 1, pp. 236–244, Jan. 2005.
- [3] A. Malik, S. Dwivedi, L. Van Landschoot, M. Muneeb, Y. Shimura, G. Lepage, J. Van, W. Vanherle, T. Van Opstal, R. Loo, and G. Roelkens, "Ge-on-Si and Ge-on-SOI thermo-optic phase shifters for the mid-infrared," *Opt. Express*, vol. 22, no. 23, pp. 28479–28488, Nov. 2014.
- [4] Y. H. Kuo, Y. K. Lee, Y. Ge, S. Ren, J. E. Roth, T. I. Kamins, D. A. B. Miller, and J. S. Harris, "Strong quantum-confined Stark effect in germanium quantum-well structures on silicon," *Nature*, vol. 437, pp.1334–1336, Oct. 2005.
- [5] G. Roelkens, U. D. U. Dave, A. Gassenq, N. Hattasan, C. Hu, B. Kuyken, F. Leo, A. Malik, M. Muneeb, E. Ryckeboer, D. Sanchez, S. Uvin, R. Wang, Z. Hens, R. Baets, Y. Shimura, F. Gencarelli, B. Vincent, R. Loo, J. Van Campenhout, L. Cerutti, J.-B. Rodriguez, E. Tournie, X. Chen, M. Nedeljkovic, G. Mashanovich, L. Shen, N. Healy, a. C. A. C. Peacock, X. Liu, R. Osgood, W. M. J. W. Green, J. Van Campenhout, and E. Tournié, "Silicon-based photonic integration beyond the telecommunication wavelength range," *J. Sel. Top. Quantum Electron.*, vol. 20, no. 4, pp. 8201511-1–8201511-9, Jul. 2014.
- [6] S. Wirths, R. Geiger, N. V. Den Driesch, G. Mussler, T. Stoica, S. Mantl, Z. Ikonc, M. Luysberg, S. Chiusi, J. M. Hartmann, H. Sigg, J. Faist, D. Buca, and D. Grützmacher, "Lasing in direct-bandgap GeSn alloy grown on Si," *Nat. Photonics*, vol. 9, no. 2, pp. 88–92, Feb. 2015.
- [7] S. Al-Kabi, S.A. Ghetmiri, J. Margetis, T. Pham, Y. Zhou, W. Dou, B. Collier, R. Quinde, W. Du, A. Mosleh, J. Liu, G. Sun, R.A. Soref, J. Tohhle, B. Li, M. Mortazavi, H. A. Naseem, and S.-Q. Yu, "An optically pumped 2.5 μm GeSn laser on Si operating at 110 K," *Appl. Phys. Lett.*, vol. 109, pp. 171105-1–171105-4, 2016.
- [8] V. Reboud, A. Gassenq, N. Pauc, J. Aubin, L. Milord, Q.M. Thai, M. Bertrand, K. Guillo, D. Rouchon, J. Rothman, T. Zabel, F.A. Pilon, H. Sigg, A. Chelnokov, J.M. Hartmann, and V. Calvo, "Optically pumped GeSn micro-disks with 16% Sn lasing at 3.1 μm up to 180 K," *Appl. Phys. Lett.*, pp. 092101, July 2017.
- [9] N. Driesch, D. Stange, D. Rainko, I. Povstugar, P. Zaumseil, G. Capellini, T. Schroeder, T. Denneulin, Z. Ikonc, J.-M. Hartmann, H. Sigg, S. Mantl, D. Grützmacher, and D. Buca, "Advanced GeSn/SiGeSn Group IV heterostructure lasers," *Advanced Sciences*, pp. 1700955, Mar. 2018.
- [10] J. Margetis, S. Al-Kabi, W. Du, W. Dou, Y. Zhou, T. Pham, P. Grant, S.A. Ghetmiri, A. Mosleh, B. Li, J. Liu, G. Sun, R.A. Soref, J. Tolle, M. Mortazavi, and S.-Q. Yu, "Si-based GeSn lasers with wavelength coverage of 2-3 μm and operating temperature up to 180 K," *ACS Photon.*, vol. 5, pp. 827–833, May 2018.
- [11] G. Z. Mashanovich, C. J. Mitchell, J. S. Penades, A. Z. Khokhar, C. G. Littlejohns, W. Cao, Z. Qu, S. Stankovic, F. Y. Gardes, T. B. Masaud, H. M. H. Chong, V. Mittal, G. S. Murugan, J. S. Wilkinson, A. C. Peacock, and M. Nedeljkovic, "Germanium mid-infrared photonic devices," *J. Lightw. Technol.*, vol. 35, no. 4, pp. 624–630, Feb. 2017.
- [12] H. Zhou, J. Sun, J. Gao, J. Jiang, and Y. Zhou, "Design of compact and efficient polarization-insensitive taper coupler for SiGe photonic integration," *Opt. Express*, vol. 24, no. 21, p. 23784–23797, Oct. 2016.
- [13] F. Xia, V. M. Menon, and S. R. Forrest, "Photonic integration using asymmetric twin-waveguide (ATG) technology: part I-concepts and theory," *IEEE J. Sel. Top. Quantum Electron.*, vol. 11, no. 1, pp. 17–29, Jan. 2005.
- [14] K. Zang, C.-Y. Lu, E. Fei, M. Xue, S. Claussen, M. Morea, Y. Chen, R. Dutt, Y. Huo, T.I. Kamins, and J.S. Harris, "Germanium quantum well QCSE waveguide modulator with tapered coupling in distributed modulator-detector system," *J. Lightw. Technol.*, vol. 35, pp.4629–4633, Nov. 2017.
- [15] M. Akie, T. Sato, M. Arai, T. Fujisawa, and K. Saitoh, "A compact and low-loss GeSn electroabsorption modulator using vertical multimode interference for mid-infrared Ge-on-Si platform," in *Conference on Lasers and Electro-Optics Pacific Rim (CLEO-PR)*, p. s1533, Jul. 31-Aug. 4 2017.
- [16] T. Fujisawa and K. Saitoh, "Material gain analysis of GeSn/SiGeSn quantum wells for mid-infrared Si-based light sources based on many-body theory," *IEEE J. Quantum Electron.*, vol.51, pp.7100108-1–7100108-8, May 2015.
- [17] T. Fujisawa and K. Saitoh, "Quantum-confined Stark effect analysis of GeSn/SiGeSn quantum wells for mid-infrared Si-based electroabsorption devices based on many-body theory," *IEEE J. Quantum Electron.*, vol. 51, no. 11, pp. 8400207-1–8400207-7, Nov. 2015.
- [18] R. Ponce, S.S. Azadeh, D. Stange, F. Merget, B. Marzban, Z. Ikonc, D. Buca, J. Witzens, "Design of a high-speed germanium-tin absorption modulator at mid-infrared wavelengths," in *Proc. IEEE Int. Conf. Group IV Photonics (GFP)*, pp. 19-20, 2017.
- [19] M. Nedeljkovic, R. Soref, and G.Z. Mashanovich, "Predictions of free-carrier electroabsorption and electrorefraction in Germanium," *IEEE Photon. J.*, vol. 7, no. 3, pp.2600214, June 2015.
- [20] M. Nedeljkovic, R. Soref, and G.Z. Mashanovich, "Free-carrier electrorefraction and electroabsorption modulation predictions for silicon over the 1.3-14 μm infrared wavelength range," *IEEE Photon. J.*, vol. 3, no. 6, pp. 1171-1180, Dec. 2011.
- [21] N. Ye, M. R. Gleeson, M. U. Sadiq, B. Roycroft, C. Robert, H. Yang, H. Zhang, P. E. Morrissey, N. Mac Suibhne, K. Thomas, A. Gocalinska, E. Pelucchi, R. Phelan, B. Kelly, J. O. Carroll, F. H. Peters, F. C. G. Gunning, and B. Corbett, "InP-based active and passive components for communication systems at 2 μm ," *J. Lightw. Technol.*, vol. 33, no. 5, pp. 971–975, Mar. 2015.
- [22] M. Koshiba and Y. Tsuji, "Curvilinear hybrid edge/nodal elements with triangular shape for guided-wave problems," *J. Lightw. Technol.*, vol. 18, no. 5, pp. 737–743, May 2000.
- [23] K. Saitoh and M. Koshiba, "Full-vectorial finite element beam propagation method with perfectly matched layers for anisotropic optical waveguides," *J. Lightw. Technol.*, vol. 19, no. 3, pp. 405–413, Mar. 2001.
- [24] T. Fujisawa and M. Koshiba, "Full-vector finite-element beam propagation method for three-dimensional nonlinear optical waveguides," *J. Lightw. Technol.*, vol. 20, no. 10, pp. 1876–1884, Oct. 2002.

- [25] T. Fujisawa, S. Kanazawa, K. Takahata, W. Kobayashi, T. Tadokoro, H. Ishii, and F. Kano, "1.3- μm , 4×25 -Gbit/s, EADFB laser array module with large-output-power and low-driving-voltage for energy-efficient 100GbE transmitter," *Opt. Express*, vol. 20, no. 1, pp. 614–620, Jan. 2012.
- [26] W. Kobayashi, K. Tsuzuki, T. Tadokoro, T. Fujisawa, N. Fujiwara, T. Yamanaka, and F. Kano, "40-Gb/s operation of 1.3/1.55- μm InGaAlAs electroabsorption modulator integrated with DFB laser in compact TO-CAN package," *IEEE Journal of Selected Topics in Quantum Electronics*, vol. 17, no. 5, pp.1183-1190, Oct. 2011.

Minami Akie was born in Sapporo, Japan, on July 8, 1993. She received the B.S. and M.S. degree in electronic engineering from Hokkaido University, Sapporo, Japan, in 2016 and 2018. She has been engaged in research on electroabsorption modulator with GeSn/SiGeSn multiple quantum well for mid-infrared photonics using finite element method. Ms. Akie is a member of the Institute of Electronics, Information and Communication Engineers (IEICE) of Japan.



Takeshi Fujisawa (M'05) was born in Sapporo, Japan, on January 12, 1979. He received the B.E., M.E., and Ph.D. degrees in electronic engineering from Hokkaido University, Sapporo, in 2001, 2003, and 2005, respectively. He was a Research Fellow of the Japan Society for the Promotion of Science from 2003 to 2006. In 2006, he joined the Nippon Telegraph and Telephone (NTT) Photonics Laboratories, NTT Corporation, Atsugi, Japan. In 2014, he became an

Associate Professor at the Graduate School of Information Science and Technology, Hokkaido University. His research interests include active optical devices for optical communication systems, such as semiconductor lasers and modulators, and theoretical modeling of optical fibers and devices. He is an author or coauthor of more than 90 papers in international refereed journals.

Prof. Fujisawa has been served as an Associate Editor of *Optics Express* from 2014 and is a Member of the Institute of Electronics, Information and Communication Engineers of Japan.

Takanori Sato (S'16-M'18) was born in Hokkaido, Japan, in 1992. He received the Ph.D. degree in the field of media and network technologies from Hokkaido University, Japan, in 2018. He has been a Research Fellow of Japan Society for the Promotion of Science since 2017. His research interests include the theoretical and numerical studies of optical fibers and photonic circuits using the coupled mode theory and the finite element method. He is a member of the Institute of Electrical and Electronics Engineers (IEEE), the Optical Society of America (OSA), and the Institute of Electronics, Information, and Communication Engineers (IEICE).

Masakazu Arai (M'96) was born in Saitama, Japan, in 1975. He received B.E., M.E., and Ph.D. degrees from Tokyo Institute of Technology, Yokohama, Japan, in 1999, 2001, and 2003, respectively. From April 2003 to March 2004, he was a Postdoctoral Scientist with the Precision and Intelligence Laboratory (P&I Lab), Tokyo Institute of Technology, where he was also engaged in the design and fabrication of vertical-cavity surface-emitting lasers. In April 2004, he joined Nippon Telegraph and Telephone (NTT) Photonics Laboratories, NTT Corporation, Atsugi, Japan. From 2016, he became an



associate professor in Miyazaki university, Japan. His current research interests include metal–organic vapor-phase epitaxy (MOVPE) growth of III–V semiconductors and the development of semiconductor lasers. Dr. Arai is a member of the IEEE Lasers and Electro-Optics Society and the Japan Society of Applied Physics (JSAP).



Kunimasa Saitoh (S'00-M'01) received the B.S., M.S., and Ph.D. degrees in electronic engineering from Hokkaido University, Sapporo, Japan, in 1997, 1999, and 2001, respectively. From 1999 to 2001, he was a Research Fellow of the Japan Society for the Promotion of Science. From 2001 to 2005, he was a Research Associate with the Graduate School of Engineering, Hokkaido University. From 2005 to 2013, he was an Associate Professor at Graduate School of Information Science and Technology, Hokkaido University, and in 2013, he became a Professor there. He has been involved in research on fiber optics, nano-photonics, integrated optical devices, and computer-aided design and modeling of guided-wave devices. He is the author of more than 190 research papers in refereed international journals and more than 240 refereed international conference presentations.

He is a Member of the Optical Society of America (OSA), and the Institute of Electronics, Information and Communication Engineers (IEICE). He was a Chair of Subcommittee D4 of Optical Fiber Communication Conference (OFC) in 2016. He is currently a Technical Program Committee of European Conference on Optical Communication (ECOC). He received the Excellent Paper Award and the Young Scientist Award from the IEICE, in 1999 and 2002, respectively, the Young Scientists' Prize of the Commendation for Science and Technology from the Ministry of Education, Culture, Sports, Science, and Technology (MEXT), Government of Japan in 2008, the JSPS Prize from the Japan Society for the Promotion of Science in 2015, and the Distinguished Lecturers Award from the IEEE Photonics Society in 2017.